Journal of The Electrochemical Society, 2023 **170** 030532

An SVM-Based Health Classifier for Offline Li-Ion Batteries by Using EIS Technology

Wei Luo, Adnan U. Syed, John R. Nicholls, and Simon Gray[z]

Cranfield University, Cranfield MK43 0AL, United Kingdom

This paper presents an offline testing framework and simulation to measure the aging situation of Li-ion batteries within the Battery Management System (BMS) or laddering use for maintenance activities. It presents the use case of Electrochemical Impedance Spectroscopy (EIS) as a non-destructive inspection method to detect battery states. Multiple cycles (charge and discharge) were done to gain EIS results in different conditions like temperature. Results were captured and digitalised through a suitable circuit model and mathematical methods for fitting. The State of Health (SOH) values were calibrated, and data were reshaped as vectors and then used as input for Support Vector Machine (SVM). These data were then used to create a machine learning model and analyse the aging mechanism of lithium-ion batteries. The machine learning model is established, and the decision boundaries are visualised in 2D graphs. The accuracy of these machine learning models can reach 80% in the test cases, and good fitting in lifetime tracking. The framework allows more reliable SOH estimation in electric vehicles and more efficient maintenance or laddering operations.

 [DOI: 10.1149/1945-7111/acc09f]

Manuscript submitted December 13, 2022; revised manuscript received February 16, 2023. Published March 24, 2023.

With the growing energy shortage and people's awareness of the environmental concept, vehicles powered wholly or partly by electricity are becoming increasingly popular among urban commuters, where lithium-ion batteries (LIBs) play a significant role as their mature manufacturing processes mature and high efficiency. Although electro vehicles (EVs) manufacturers have been developed many charging and discharging strategies and monitoring measures to prolong better batteries' lifetime, the bias between the estimated mileage onboard and actual mileage is expected to grow over time, which is a visual reflection of the declining battery state of health (SOH) and capacity fade. This affects the driver's judgment of the car's condition, even though the actual measured capacity loss is less than 20%, a threshold for EV batteries to be replaced or scrapped. This is also limited to cars like Tesla that are well-equipped with various sensors and high-performance CPUs to monitor and estimate battery status. It will be worse for early EVs or vehicles with less sensors.

At the same time, due to long charging times, some manufacturers are now pushing the battery swap mode to allow further echelon utilisation of batteries as the replacement batteries are collected in the battery switching station. A. Q. Pan and X. Z. Li[1] discussed that the EV decommissioned batteries still have great echelon use-value. They can be reintegrated into a distributed energy storage system to extend their service life. The main hindrance to this mode is that people cannot get an intuitive sense of the health of the battery they have purchased compared to the original one unless they have used them for a period until the state-of-the-art BMS can calibrate and estimate an updated SOH. Therefore, no matter charging or battery swapping and recycling, a reliable, low power requirement and super-fast battery health monitoring method compatible with most battery management systems without relying on historical data are essential.

A standard method of SOC estimation is through the OCV-SOC curve,[2] which is an empirical curve and has the advantage of being fast and accurate for SOC estimation of batteries with significant variations in OCV. However, in SOH estimation, methods based purely on DC resistance tend to be progressively less accurate in changing charge/discharge configurations, so resistance-based SOH estimation methods need to be improved.

Increases in internal resistance are a visual reflection of capacity decreases, influenced by various phenomena of electrochemical reactions within the battery. Therefore, electrochemical impedance spectroscopy (EIS) provides a non-destructive battery diagnostic. By applying a sinusoidal current or voltage signal, the impedance can be calculated by Ohm's Law in AC circuits. Such technology will be discussed in the following section.

It is not the only case where people have been integrating EIS into the battery management system. For example, Bliss G. Carkhuff's team[3] has developed an impedance-based battery management system that includes monitoring of cell voltage, surface temperature, electrolyte resistance, and GEIS testing module, which is able to measure the frequency range from 1 Hz to 1 kHz with the phase resolution up to 0.0123°. The appearance of an impedance-based battery management system has undoubtedly increased SOH estimation reliability.

Previously, several studies have explored how EIS[4–11] can be used to determine or evaluate batteries' SOH. Still, some have only looked at the effect of cycle count on battery ageing. Alarm Eddahech et al.[12] have been tried to identify the behaviour and monitor SOH using EIS and recurrent neural networks combined the SEI resistance with charge transfer resistance into equivalent series resistance (ESR) and have not analysed them separately due to the equivalent circuit model (ECM) that have been adopted. Other studies, such as the algorithm developed by Xin Zhou et al.[11] are difficult to be integrated into an already designed BMS due to their complexity and a large amount of power consumed to train the neural network model. Artificial neural network-based methods require the system to be switched on for an extended period to ensure the model can be trained continuously for each cell,[13] and high computational costs are also required.[7,11–14] This article provides a relatively easy and low computational cost machine learning method to determine the health status of SamSung 18 650 batteries by referring to similar behaviours of the same model, considering factors such as temperature.

Electrochemical Impedance Spectroscopy (EIS)

The most straightforward and widely adopted method for the capacity diagnostic is coulomb counting or the Ampere-Hour method in another name.[15] The capacity can be estimated according to the electric quantity delivered and the differences in the state of charge (SOC) between the two points. This method can be further extended to the multi-point regression method using the least square algorithms. The accuracy of conventional methods relies heavily on the accuracy of SOC estimates. But fortunately, with the widespread use of tools such as Kalman filtering, SOC estimation has become entirely accurate, so the SOH acquired from this method is the most

[z]E-mail: s.gray@cranfield.ac.uk

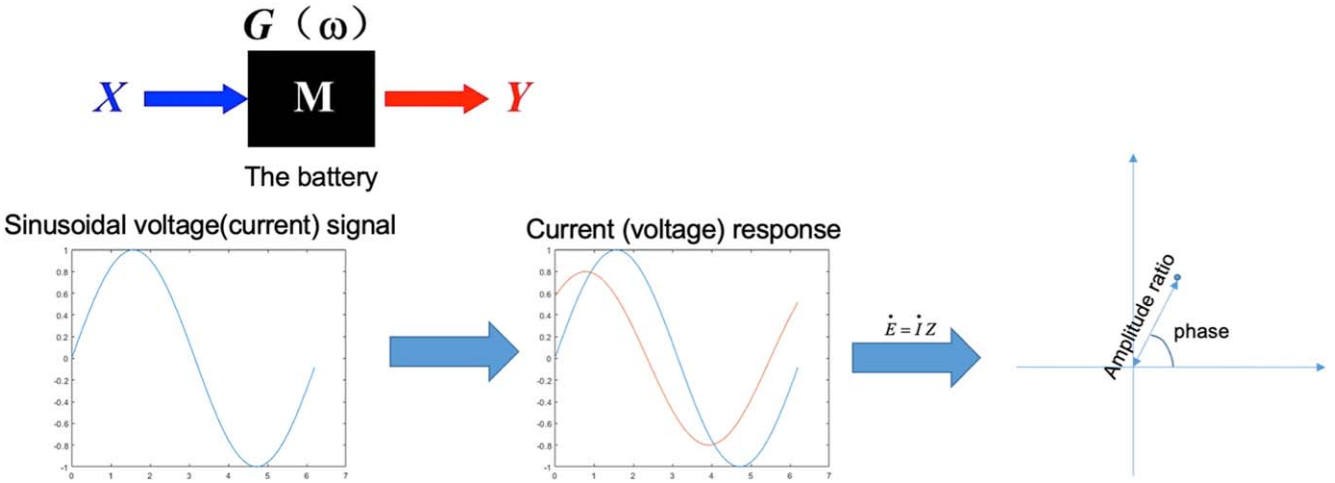

Figure 1. EIS Principal.

accurate. However, the biggest problem with this method remains the extended testing time. According to ISO 12405, the energy performance test should be conducted under 1C when discharging, which means it will take 55–60 min to acquire the SOHs.

The above methods are all based on the externalisation of the cells to determine their level of ageing, which means that the cells must exhibit a specific electrical performance when powering. The EIS, on the other hand, provides a microscope-like view of the battery's condition without the need to disassemble the batteries or place the electrodes directly under the SEM. This also means that the batteries can be measured or supervised, whether they are in up-time or not and whether they are running at a high or low temperature. The principle of EIS can be described in Fig. 1.

A sinusoidal voltage or current signal is applied to the poles of the battery over time. Different currents flowing through the battery produce a specific voltage drop and vice versa. As a result, their images are accompanied by a delay or overrun of the phase. By scanning a particular frequency range one by one and recording the amplitude and phase changes of the response, a Nyquist plot and a Bode plot can be obtained. A Nyquist plot can be divided into three-part, the high-frequency region, the medium frequency region, and the low-frequency region, representing the different electrochemical reactions within the cell.[16] The meaning of each part is shown in Fig. 2.

Depending on the type of the input signal, the EIS can be divided into Potential EIS (PEIS) and Galvano EIS (GEIS), where PEIS applies a sinusoidal voltage signal, and GEIS uses a sinusoidal current signal. A review is done by N. Meddings et al.[17] discussed the pros and cons of using PEIS and GEIS in commercial batteries. As commercial cells have much lower impedance than lab-scale cells, a large output current flow will be generated by small input voltage perturbations. Therefore, high current perturbation (GEIS) is recommended when accurate measurement results are required, as the increase in internal temperature brings less impact. However, PEIS, although its Nyquist plot is not always strictly linear in the low-frequency region due to its low signal interference, is still widely used.[18]

Machine learning-based predictor.—As EIS results may be varied due to the high sensitivity of the technique and non-linear relationships between each variable, both well-trained machine-learning or artificial neural network (ANN) models offer these same targets an explicit boundary to blur the allowed inputs to ensure different predictions will appear only when the inputs differ significantly, as shown in Fig. 3.

Machine learning and ANN are aiming at solving the classification problem. This study will be based on the support vector machine (SVM).

SVM is a commonly used supervised machine learning approach, and thanks to the addition of the kernel function, non-linearly divisible data sets can also be classified typically.

The essence of SVM lies in partitioning the scatter points in a scatter plot projected in n-dimensional space as evenly as possible utilizing optimal hyperplanes. These hyperplanes will form models that can be used to estimate scatter points get from other sources. These hyperplanes can be described as:

$$w^T x + b = 0 \quad [1]$$

The process of solving the SVM lies in finding the above hyperplane coefficients:

$$\min \frac{1}{2}\|w\|^2 \quad s.t. y_i(w^T x_i + b) \geqslant 1 \quad [2]$$

In practice, fully linearly divisible samples are rare. If the sample is not fully linearly separable, a soft margin can be designed to allow a few individual samples to appear in the margin bands. Then the Eq. 2 can be expanded to:

$$\min \frac{1}{2}\|w\|^2 + C\sum_{i=1}^{m} \xi_i s.t. g_i(w, b) = 1 - y_i(w^T x_i + b)$$
$$-\xi_i \leqslant 0 \quad \xi_i \geqslant 0, \quad i = 1, 2, \ldots, n \quad [3]$$

Where $\xi_I \geqslant 0$.

C is a constant greater than 0, which can be interpreted as the intense penalty for incorrect samples. If C is infinite, ξ_i must be

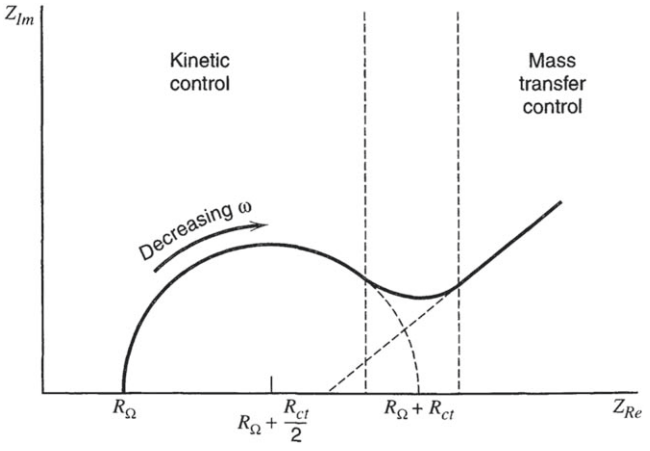

Figure 2. Referred Chemical Reactions in Nyquist Plots.

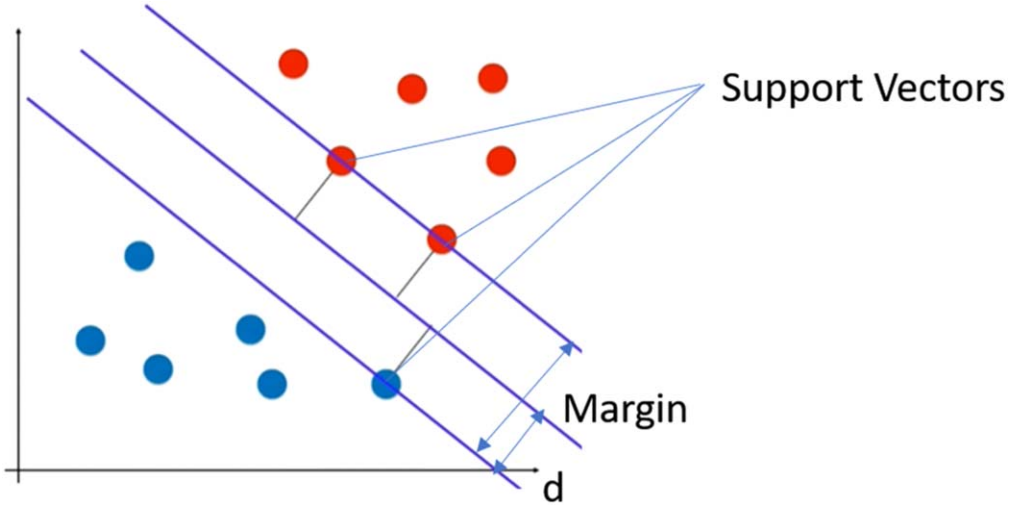

Figure 3. Explicit Boundary for SVM.

infinitely small, and then the problem will go back to the hard margin Eq. 2. Only when C is a finite value will some samples be allowed not to follow the constraints.

Experimental

Circuit for multiple channels EIS measurement.—EIS method is relatively straightforward. Cells can be measured by directly connecting their two electrodes to the electrochemistry workstation. However, current equipment in the market only provides a single channel for EIS measurement. Since the AC properties. Since the measurement signal is AC voltage (PEIS) or current (GEIS), the generated alternating magnetic field is easily disturbed by external electromagnetic waves, making the curve fluctuate during the measurement process, resulting in bad fitting results.

In order to test multiple cells at the same time as well as make them compatible within a BMS, a relay board controlled by Raspberry Pi was introduced in the experiment. Each relay was used as a switch to ensure that only one cell would be connected to the EIS measuring equipment at any one time. However, Fig. 4 shows Nyquist plots generated from the same cell. The only difference between them is whether they are connected to the relay via other wires, as the curves from the Bode graph are almost parallel (Fig. 5). It indicates that due to the high sensitivity of the EIS technique and the similarity of the cell and wire resistance values (tens of milliohms), the semicircles in the Nyquist plot will produce light changes in diameter significant overall curve biases, leading to the inconsistency of training dataset.

To address this issue, a circuit was designed as Fig. 6. Two relays are connected on both sides of the battery, and all wires are twisted pairs to avoid the influence of adjacent channels and external waves. The positive and negative buses are connected to holes in the two terminals to ensure that each battery reaches the EIS measuring equipment through the same number of holes leading to the same terminal resistances. The wire used between batteries and relays are twisted pairs, and the shield leads are connected to the normally open output. All normally available outputs have joined each other to the ground to ensure that the test signal is not distorted. After applying the circuit, the EIS results of the same battery in different channels became consistent, and the example table below can compensate for the differences.

Cells information.—The cells used in the experiment are SamSung ICR18650–26J. The nominal capacity is 2,600 mAh (25 °C, 3.7 V). According to the datasheet from SamSung, other technical details and ageing profiles are shown in Tables I and II.

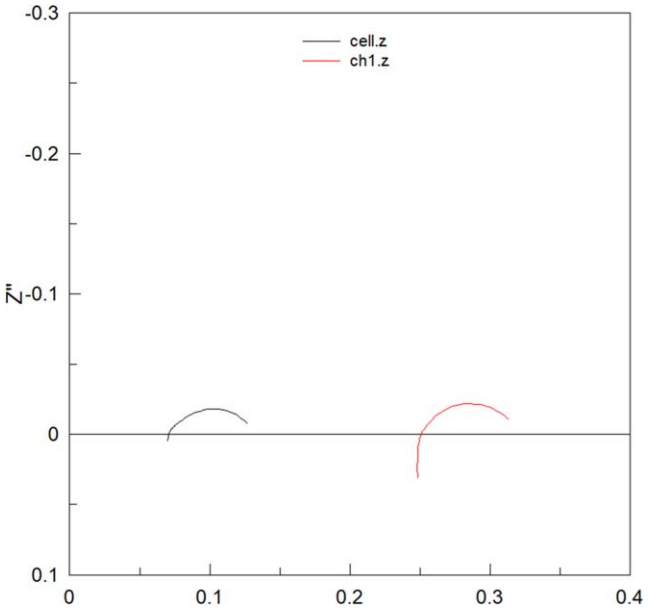

Figure 4. Nyquist Plots Differences caused by DC elements.

As shown in Table II, the amount of energy released and charged in a single cycle is highly dependent on the ambient temperature. When the cell is fully charged under 25 °C, it can be discharged 50% of nominal capacity at 0.2C under −10 °C, 70% under 0 °C, and 95% under 45 °C, respectively. On the contrary, when the cell is fully discharged under 25 °C, and charge with Constant Current (CC)-Constant Voltage (CV) method. The cell can only be charged 80% of nominal capacity until it reaches the maximum charging voltage under 0 °C.

Test matrix and experimental procedure.— *Environment selection.*—Although electrochemical reactions are also affected by humidity, in the case of finished, commercial batteries, as the reactants are encapsulated in a shell that insulates them from water vapour, the effect of moisture on them will be relatively small, as the preceding experiments have demonstrated.

Therefore, two temperature levels of 10 °C and 25 °C were set within the permissible range, according to the instructions in Table I. At these two temperature levels, the relative humidity is always maintained at 50% (±5%).

The selected environments are shown in Table III.

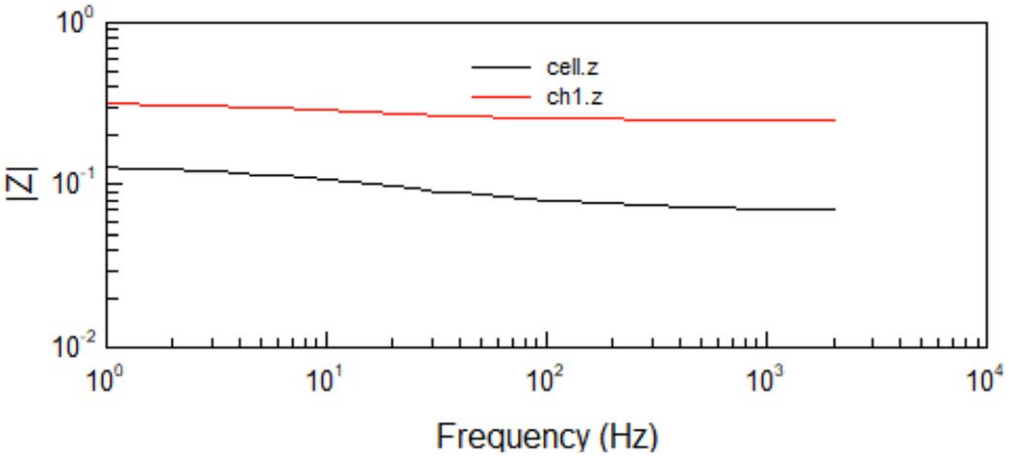

Figure 5. Bode Plots Differences caused by DC elements.

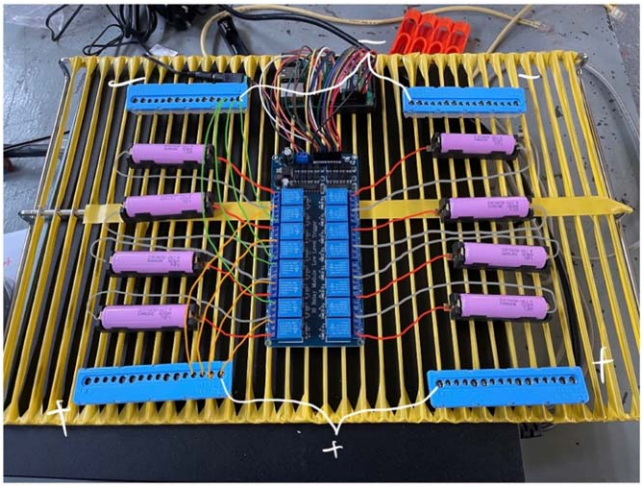

Figure 6. Multiple Channels for EIS.

Experimental procedure.—The experiment flow chart is shown in Fig. 7. Before the start of each temperature level start, the circuit shown in Fig. 6. must be calibrated to eliminate the effects of wire resistance. This is done by using the same cell for one test on each channel and then performing another test without access to the circuit. The difference in R_{Ω} obtained is the line resistance value, which needs to be removed in subsequent processing.

After the calibration was completed, 12 cells were placed at each temperature, which had undergone three cycles to achieve activation at the start of the experiment. Using CC–CV (1C) as the charging profile and CC (2C) as the discharging profile, the batteries were left to rest for 20 min after every 20 discharge-charge cycles. Next, the EIS test was performed on each cell placed in the channel, recording data to generate values for each element at that temperature and for that number of cycles. Once the tests were completed, the energy released by each of them was recorded using the Ampere-Hour method of fully discharge, completing the SOH calculation as a target to be estimated for machine learning. After completing the test, continue with the charge/discharge experiment and wait for the subsequent 20 cycles to complete. All cells will be stopped testing when their SOH drop below 50%.

Table I. Cell Information for Samsung ICR 18650–26 J.

Nominal Capacity	2600 mAh (0.2C, 2.75 V discharge)
Charging Voltage	4.2 ± 0.05 V
Nominal Voltage	3.7 V
Maximum Charge Current	2600 mA
Maximum Discharge Current	5200 mA
Discharge Cut-off Voltage	2.75 V
Operating Temperature	Charge: 0 °C to 45 °C
	Discharge: −20 °C to 60 °C

Temperature Dependence.

Models and tools.— *Equivalent circuit model.*—Equivalent circuit models are made based on the experimental results representing the behaviour of a Li-ion cell in response to different techniques. In EIS, they refer to the structure of the electrode and electrolyte.

This section explains the basic formula for the EIS fitting using a resistor R in series with an RC parallel circuit as the elemental composition within a battery. However, when a cell is being aged, another RC circuit will represent the characteristic brought by the SEI layer.The simplified microstructure of ECM are defined in Figure 8.

The following equivalent circuit diagram can simplify the chart above:

Where:

R_{Ω} - Solution (Ohmic) resistance

R_{sei} - SEI layer resistance

R_{ct} - Polarisation (Charge transfer) resistance

C_{d1} - Double layer capacitor (between solution and SEI layer)

C_{d2} - Double layer capacitor (between SEI layer and electrodes)

Table II. Temperature Dependences of Samsung ICR 18650–26 J.

Charge Temperature			Discharge Temperature	
25 °C	−10 °C	0 °C	25 °C	45 °C
Relative Capacity	50%	70%	100%	95%
		Charge temperature		Discharge temperature
	0 °C	25 °C	45 °C	25 °C
Relative Capacity	80%	100%	100%	

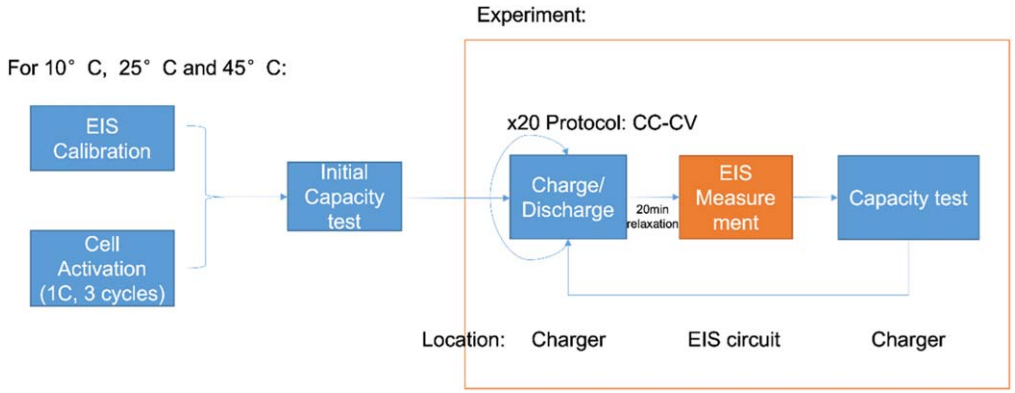

Figure 7. Experiment Settings.

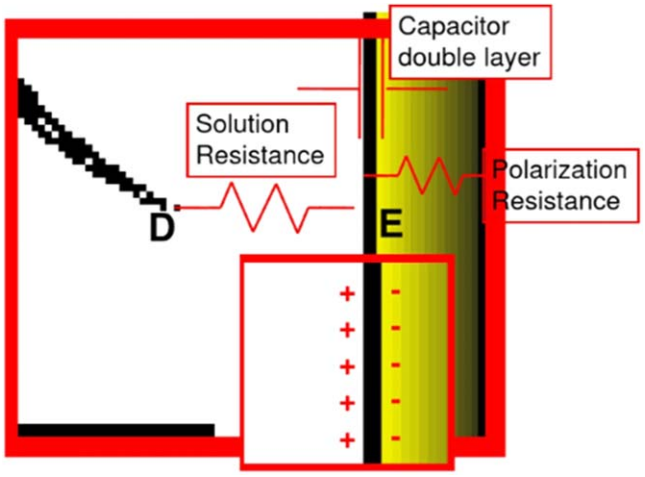

Figure 8. Simplified Microstructure of Li-ion Batteries Electrodes.

Despite the Warburg resistance at the end. The impedance of the equivalent circuit above at this point:

$$\begin{aligned} Z &= R_\Omega + \frac{1}{jwC_{d1} + \frac{1}{R_{sei}}} + \frac{1}{jwC_{d2} + \frac{1}{R_{ct}}} \\ &= R_\Omega + \frac{R_{sei}}{1 + w^2C_{d1}^2 + R_{sei}^2} + \frac{R_{ct}}{1 + w^2C_{d2}^2 + R_{ct}^2} \\ &\quad - j\frac{wC_{d1}R_{sei}^2}{1 + w^2C_{d1}^2 + R_{sei}^2} - j\frac{wC_{d2}R_{ct}^2}{1 + w^2C_{d2}^2 + R_{ct}^2} \end{aligned} \quad [4]$$

In the equation above, the resistance part brought by SEI resistance satisfy:

$$\left(Z_{\mathrm{Re}(sei)} - R_\Omega - \frac{R_{sei}}{2}\right)^2 + Z_{\mathrm{Im}(sei)}^2 = \left(\frac{R_{sei}}{2}\right)^2 \quad [5]$$

The coordinate of the SEI circle is $\left(R_\Omega + \frac{R_{sei}}{2}, 0\right)$ and a radius of $\frac{R_{sei}}{2}$. Similarly, the radius of charger transfer resistance can be $\frac{R_{ct}}{2}$, and they are connected at the beginning and end.

Impedance fitting automation.—The above calculation can be simplified and automated by Impedance.py, whose equivalent circuit can be described as follows, according to Fig. 9:

$$R_0 - p(R_1, C_1) - p(R_2 - W_{01}, C_2) \quad [6]$$

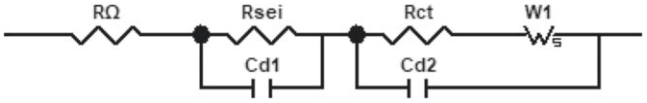

Figure 9. Equivalent Circuit for EIS Fitting.

Table III. Selected Environments.

Temperature	10 °C	25 °C
Relative humidity (±5%)	50%	

Where:

$$\begin{cases} R_0 = R_\Omega \\ R_1 = R_{sei} \\ R_2 = R_{ct} \end{cases} \begin{cases} C_1 = C_{d1} \\ C_2 = C_{d2} \end{cases} \quad [7]$$

To fit correctly, initial guesses also need to be set, which can be obtained using the instant fit function in the Zview software. In this case, for SamSung ICR18650–26j, the initial guesses are defined in Table IV:

Validation.—This section is based on a pre-experiment that only considered the EIS curve changes with the cycle number. A single cell was put in a room where the temperature and relative humidity did not change significantly. The cell was cycled (charge and discharge) at 2 A and. After the 1st, 30th and 50th cycles, EIS was applied ten times and recorded the value of ohmic resistance, SEI resistance and charge transfer resistance to generate training data. The SEI resistance arc began to show up during charging and discharging, and the charge transfer resistance continuously increased within these 50 cycles. In contrast, the ohmic resistance changed when the cell was activated (Figs. 10 and 11).

The results of the pre-experiments are satisfactory, but this is far from the limits of machine learning. For example,[19] showed how temperature affected charge transfer resistance and gave a conversion formula for charge transfer resistance in different temperatures. At the same time,[20] revealed that relative humidity is a long term factor that changes the value of SEI resistance. From the conclusion of Ref. 20, it is clear that commercial lithium batteries will be less affected by humidity during cycling due to good packaging. This study's objective is to determine the SOH value by the corresponding relationship between a set of resistances and capacity released developed by machine learning.

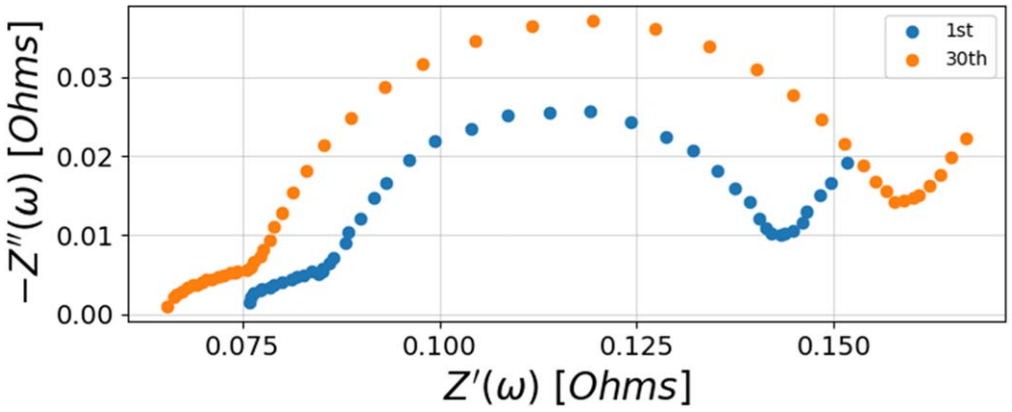

Figure 10. EIS comparison (1st vs 30th).

Vectors forming.—For the SVM algorithm, each input data must contain at least two features and the target value for estimation. The values of the features can be the values of each element in the equivalent circuit model. In the traditional sense, SOH values are given in 1% intervals. However, from the SVM point of view, datasets that are too dense and have too much similarity between adjacent targets (due to fitting and experimental errors) are likely to have a detrimental effect on the accuracy of the estimates. Therefore, a further narrow down assessment of the targets is required. In this case, the SOH values can be compressed to an interval of 10% by using the following criteria:

Using the criteria above, it can be deduced that if the machine learning results are correct, the error can be controlled to within 10%. At this point, the vectors used for machine learning can be shown as follows:

SVM predictor.—After obtaining the values of the elements of the equivalent circuit above, the SVM optimisation problem for SOH estimation can be obtained by combining Eqs. 8 and 9:

$$w^T E + b = 0 \qquad [8]$$

$$\min_{\omega} \frac{1}{2} \|w\|^2 + C \sum_{i=1}^{m} \xi i$$
$$s.t. g_i(w, b) = 1 - SOH_{target}(w^T Ei + b)$$
$$- \xi i \leqslant 0, \xi i \geqslant 0, i = 1, 2, ..., n \qquad [9]$$

Where:

$$E = (R_0 \quad R_1 \quad C_1 \ ...)$$

$$SOH_{target} = (10.95 \quad 0.85 \quad 0.75 \ ... \ 0.45)$$

So far, by taking the values of each element obtained for different cells at each stage and matching them with their SOH values, an SVM model for SOH estimation can be obtained, and this model can be used to estimate the SOH of future cells.

Results

This chapter shows the results of all the above operations, which includes (a) fitting results, (b) machine learning results. The analysis will focus on the EIS results because their analysis results determine whether the algorithm can learn how the lithium-ion battery aging.

Fitting results.—This section shows the fitting results of "impedance.py." As shown in Figs. 12 and 13, 12 fitting curves from 1st and 30th cycles respectively are all able to fit the two arcs shown in original data. Thus, the resistance or each resistor can replace an entire curve in the original data to some extent, making the curve digitised in order to become inputs in machine learning.

Machine learning results.—The SVM boundary plots at 10 and 25 degrees are shown in Figs. 14 and 15, where the original training data showed in dots with Rsei, Rct and SoH, with the machine learning results in background colours.

In Figs. 14 and 15, each dot refers to one piece of data, with Rsei and Rct as different resistance and its colour indicates the SoH at this time. The colour regions showed the machine learning results under specific temperature level. By referring to plots like Figs. 14 and 15, a quick decision about an unknown cell's SoH can be made only if a fast EIS diagnosis can be applied. The boundaries at 10 °C and 25 °C showed different ageing patterns, which may contribute inferring other machine learning results under other non-experimental temperatures. This will be discussed in the next chapter.

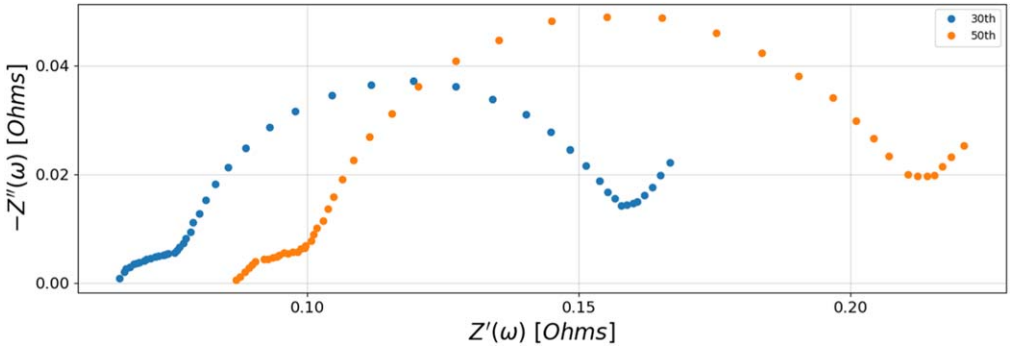

Figure 11. EIS comparison (30th vs 50th).

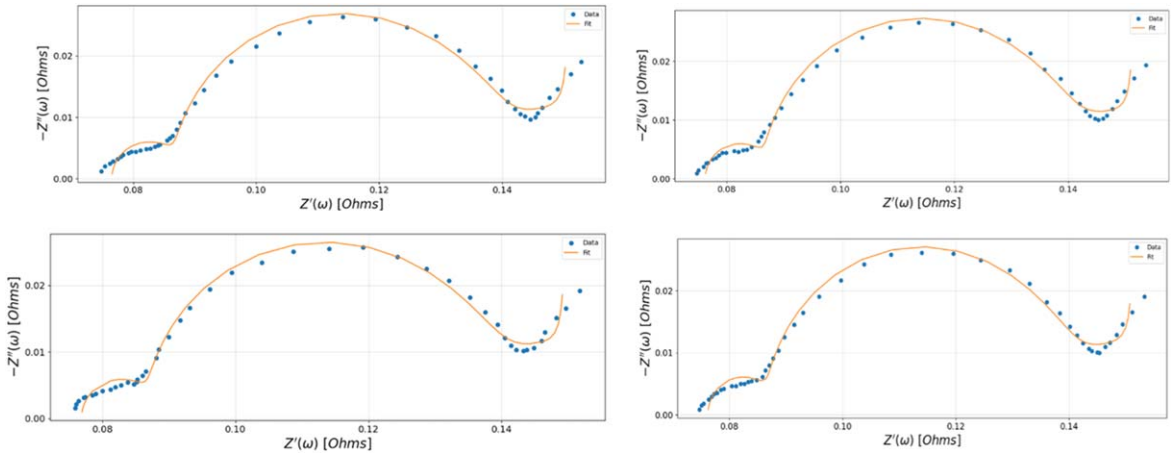

Figure 12. Fitting Results after the 1st Cycle.

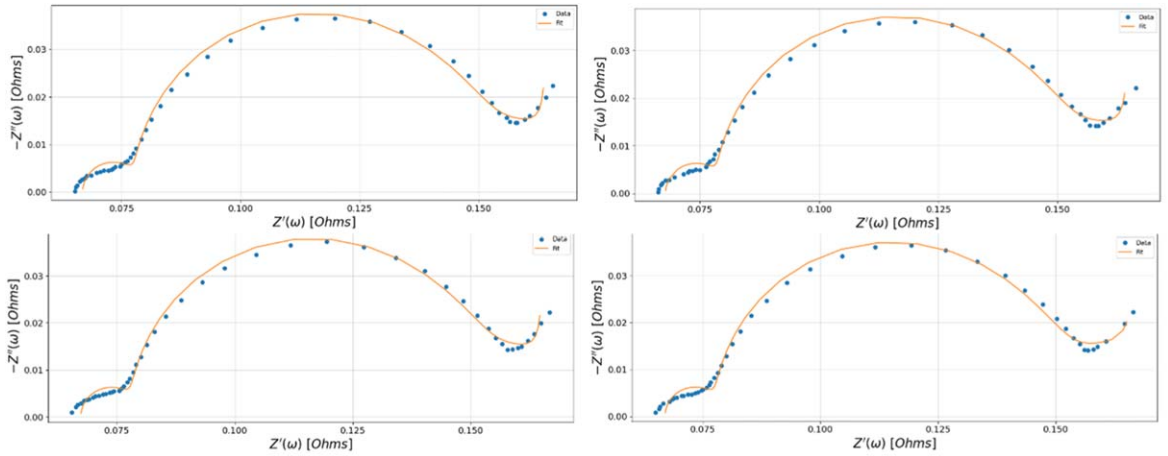

Figure 13. Fitting Results after the 30th Cycle.

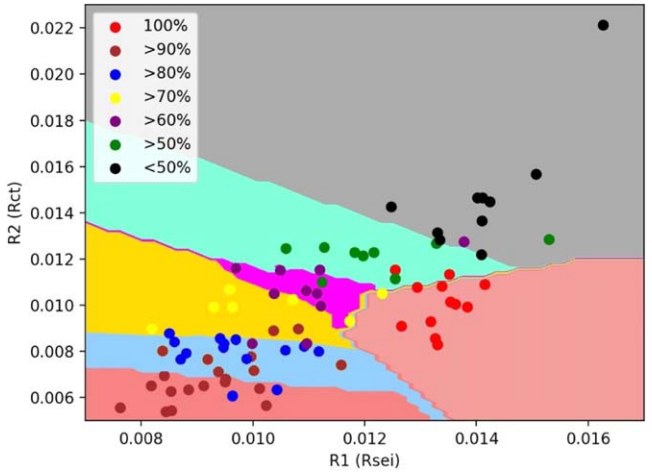

Figure 14. Boundary plot for 10 °C (Rsei vs Rct).

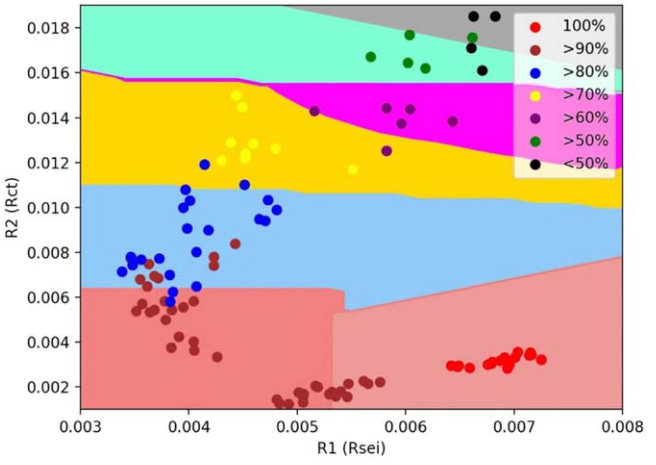

Figure 15. Boundary plot for 25 °C (Rsei vs Rct).

Discussion

SOH estimation for unknown cells.—It is easy to see from the visualised model (Figs. 14 and 15) that the boundaries at 10 °C tend to be at an angle to the *x*-axis, while the boundaries at 25 °C tend to be several parallel lines. This means that the capacity decay at 10 °C tends to depend on the joint growth of Rsei and Rct. In contrast, the capacity decay at 25 °C depends mainly on the growth of Rct, which is the same conclusion as that obtained from previous battery ageing experiments.

In this case, the entire dataset can be split randomly into two, with 70% being used for model training of the SVM and 20% for validation of the model's generalisation ability.

By putting the test set into the model, an estimate from machine learning can be obtained, which can be compared with the results obtained from the Ampere-Hour method to give the model's

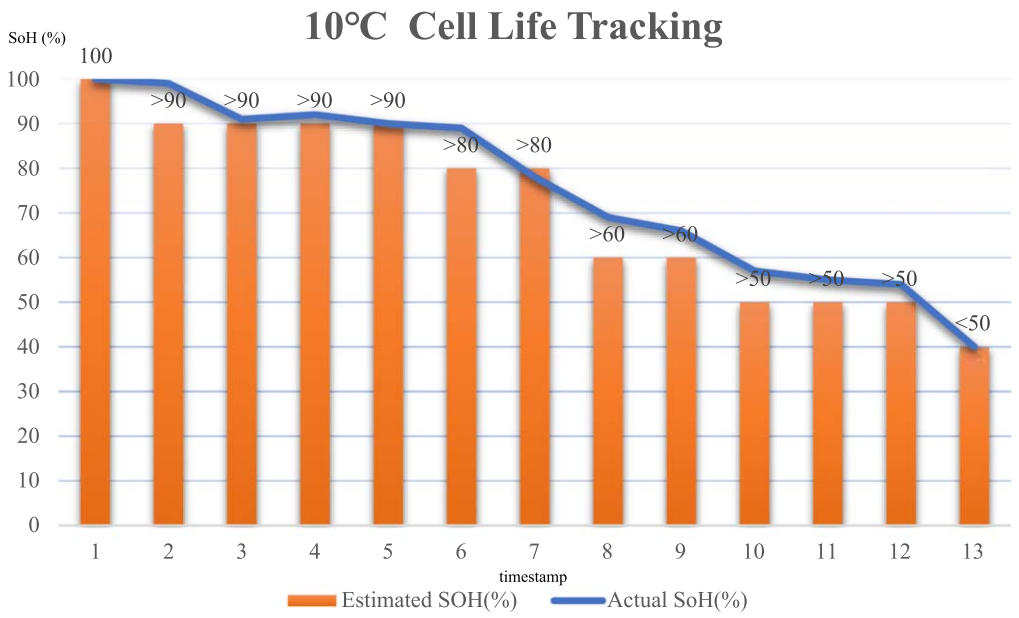

Figure 16. Life Tracking under 10 °C.

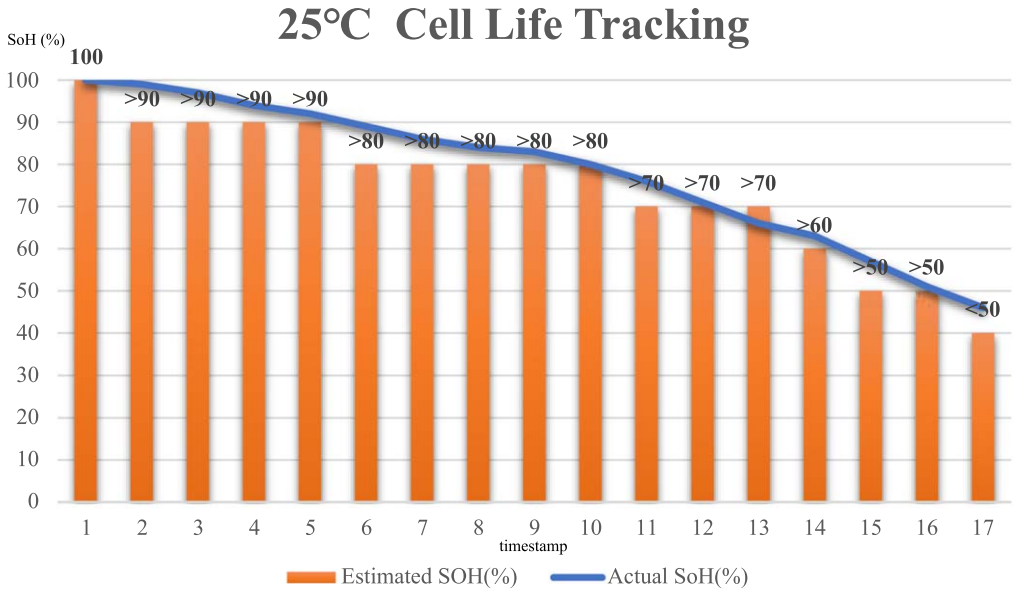

Figure 17. Life Tracking under 25 °C.

Table IV. Initial guesses for fitting.

Elements	Initial guess
R0	0.1
R1	0.001
C1	0.1
R2	0.001
C2	1
W1_0	0.001
W1_1	1

Table V. SOH narrow down criteria.

SOH range	SOH estimate target
100%	>99%
90%–99%	>90%
80%–89%	>80%
70%–79%	>70%
60%–69%	>60%
50%–59%	>50%
<50%	<=50%(failed)

accuracy. The selected data in 10 °C and 25 °C and the machine learning results based on these selected data are shown in Table VII and Table VIII, with the correct answers listed at the last column. :

After several training sessions, the model's accuracy can reach over 80% at both 10 °C and 25 °C, proving that the model has good generalisation ability.

Table VI. Vector Example.

R0	R1	C1	R2	….	SOH target

Table VII. Result of estimation for Random-Selected Cells (10 °C).

SOH Data (%)	Target Answer (%)	Estimated Answer (%)
46	<50	<50
85	>80	>80
72	>70	>70
67	>60	>60
98	>90	100
76	>70	>70
38	<50	<50
100	100	100
100	100	100
99	>90	100
83	>80	>80
60	>60	>60
95	>90	>90
55	>50	>50
40	<50	<50

Table VIII. Result of estimation for Random-Selected Cells (25 °C).

SOH Data (%)	Target Answer (%)	Estimated Answer (%)
91	>90	>90
97	>90	>90
98	>90	100
93	>90	>90
100	100	100
94	>90	>90
100	100	100
84	>80	>80
100	100	100
86	>80	>80
72	>70	>70
88	>80	>80
83	>80	>80
90	>90	>80
75	>70	>70
76	>70	>70
46	<50	<50
56	>50	>50
97	>90	>90
89	>80	>80
84	>80	>80

Lifetime tracking.—By focusing on the lifetime of a particular cell, the machine learning estimation can be obtained and see how they changed by the actual SOH, shown in Figs. 16 and 17.

From the figures, it can be seen that in the estimation for the battery lifetime, the machine learning estimates have a high fit to the actual SOH, demonstrating the robustness of this machine learning model in estimating SOH.

Conclusions

This paper presents an offline SOH estimation method based on an equivalent circuit approach, using EIS measurements combined with machine learning, especially SVM. This machine learning model provides an accurate description of Li-ion battery cell aging, taking some critical phenomena in cell reaction into account, such as temperature dependence and internal resistance. The model can reveal an accurate SOH range without taking any charge/discharge action or any historical data in a short time compared to other SoH algorithms (Figure 18). The verification was done by randomly selecting data from the whole dataset and comparing the actual SOH and the machine learning estimation.

Tests at different temperatures reveal the relationship between the loss of capacity and the increase of different components within the internal resistance. The SVM based SOH indicator provides a simulation on Li-ion battery aging behaviour in various temperature levels, taking all components in the ECM into account. This indicator can be used in applications such as the laddering of lithium batteries and the initial estimation of SOH in the battery management system where rapid diagnosis is required. These encouraging simulations represent an initial contribution to the development of offline battery aging monitoring and SOH estimation.

ORCID

Wei Luo https://orcid.org/0000-0002-9066-1077
Adnan U. Syed https://orcid.org/0000-0003-1650-9197
Simon Gray https://orcid.org/0000-0003-1265-0759

References

1. A. Q. Pan et al., "The applications of echelon use batteries from electric vehicles to distributed energy storage systems." *IOP Conf. Ser.: Earth Environ. Sci.*, **354**, 3 (2019).
2. C. Zhang, J. Jiang, L. Zhang, S. Liu, L. Wang, and P. C. Loh, "A generalized SOC-OCV model for lithium-ion batteries and the SOC estimation for LNMCO battery." *Energies*, **9**, 3 (2016).
3. B. G. Carkhuff, P. A. Demirev, and R. Srinivasan, "Impedance-based battery management system for safety monitoring of lithium-ion batteries." *IEEE Trans. Ind. Electron.*, **65**, 6497 (2018).
4. P. Liu, W. Zhang, X. Liu, Y. Zhang, and F. Wu, "Electrochemical impedance analysis of C/LiFePO4 batteries in cycling process." *IOP Conf. Ser.: Mater. Sci. Eng.*, **452**, 2 (2018).
5. J. Jiang, Z. Lin, Q. Ju, Z. Ma, C. Zheng, and Z. Wang, "Electrochemical impedance spectra for lithium-ion battery ageing considering the rate of discharge ability." *Energy Procedia*, **105**, 844 (2017).
6. D. I. Stroe, M. Swierczynski, A. I. Stroe, S. K. Kaer, and R. Teodorescu, "Lithium-ion battery power degradation modelling by electrochemical impedance spectroscopy." *IET Renew. Power Gener.*, **11**, 1136 (2017).
7. Y. Zhang, Q. Tang, Y. Zhang, J. Wang, U. Stimming, and A. A. Lee, "Identifying degradation patterns of lithium ion batteries from impedance spectroscopy using machine learning." *Nat. Commun.*, **11**, 6 (2020).
8. J. Schmitt, A. Maheshwari, M. Heck, S. Lux, and M. Vetter, "Impedance change and capacity fade of lithium nickel manganese cobalt oxide-based batteries during calendar aging." *J. Power Sources*, **353**, 183 (2017).
9. D. I. Stroe, M. Swierczynski, A. I. Stroe, V. Knap, R. Teodorescu, and S. J. Andreasen, "Evaluation of different methods for measuring the impedance of lithium-ion batteries during ageing." *2015 10th Int. Conf. Ecol. Veh. Renew. Energies, EVER 2015* (2015).
10. D. Stroe, M. Swierczynski, A. I. Stan, R. Teodorescu, and S. J. Andreasen, "Experimental investigation on the internal resistance of Lithium iron phosphate battery cells during calendar ageing." *IECON Proc. (Industrial Electron. Conf.* 6734 (2013).
11. X. Zhou and J. Huang, "Impedance-based diagnosis of lithium ion batteries: identification of physical parameters using multi-output relevance vector regression." *J. Energy Storage*, **31**, 101629 (2020).
12. A. Eddahech, O. Briat, N. Bertrand, J.-Y. Delétage, and J.-M. Vinassa, "Behavior and state-of-health monitoring of Li-ion batteries using impedance spectroscopy and recurrent neural networks." *Int. J. Electr. Power Energy Syst.*, **42**, 487 (2012).
13. A. Nuhic, T. Terzimehic, T. Soczka-Guth, M. Buchholz, and K. Dietmayer, "Health diagnosis and remaining useful life prognostics of lithium-ion batteries using data-driven methods." *J. Power Sources*, **239**, 680 (2013).
14. M. Bezha and N. Nagaoka, "A fast diagnosis for classification of re-used Li-ion batteries for PV and EV systems by the ANN model." *2019 IEEE 8th Glob. Conf. Consum. Electron. GCCE 2019*1139 (2019).
15. K. S. Ng, C.-S. Moo, Y.-P. Chen, and Y.-C. Hsieh, "Enhanced coulomb counting method for estimating state-of-charge and state-of-health of lithium-ion batteries." *Appl. Energy*, **86**, 1506 (2009).

16. A. J. Bard and L. R. Faulkner, *Electrochemical Methods Fundamentals and Applications*. (New York, Wiley) 2nd ed., Vol 2 (2001).
17. N. Meddings et al., "Application of electrochemical impedance spectroscopy to commercial Li-ion cells: A review." *J. Power Sources*, **480**, 3 (2020).
18. H. Tian, P. Qin, K. Li, and Z. Zhao, "A review of the state of health for lithium-ion batteries: Research status and suggestions." *J. Clean. Prod.*, **261**, 120813 (2020).
19. X. Wang, X. Wei, and H. Dai, "'Estimation of state of health of lithium-ion batteries based on charge transfer resistance considering different temperature and state of charge,'." *J. Energy Storage*, **21**, 618 (2019).
20. S. Byun, J. Park, W. A. Appiah, M.-H. Ryou, and Y. M. Lee, "The effects of humidity on the self-discharge properties of Li (Ni 1/3 Co 1/3 Mn 1/3) O 2/graphite and LiCoO 2/graphite lithium-ion batteries during storage." *RSC Adv.*, **7**, 10915 (2017).

An SVM-based health classifier for offline Li-ion batteries by using EIS technology

Luo, Wei

2023-03-24

Luo W, Syed AU, Nicholls JR, Gray S. (2023) An SVM-based health classifier for offline Li-ion batteries by using EIS technology. Journal of The Electrochemical Society, Volume 170, March 2023, Article number 030532

https://doi.org/10.1149/1945-7111/acc09f